Three-dimensional micro assembly of a hinged nickel micro device by magnetic lifting and micro resistance welding

2009 J. Micromech. Microeng. 19 105026

(http://iopscience.iop.org/0960-1317/19/10/105026)

J. Micromech. Microeng. **19** (2009) 105026 (8pp) doi:10.1088/0960-1317/19/10/105026

Three-dimensional micro assembly of a hinged nickel micro device by magnetic lifting and micro resistance welding

Chun-Wei Chang and Wensyang Hsu[1]

Department of Mechanical Engineering, National Chiao Tung University, 1001 Ta Hsueh Road, Hsinchu, 30010, Taiwan, Republic of China

E-mail: whsu@mail.nctu.edu.tw

Received 14 May 2009, in final form 14 July 2009
Published 22 September 2009
Online at stacks.iop.org/JMM/19/105026

Abstract

The three-dimensional micro assembly of hinged nickel micro devices by magnetic lifting and micro resistance welding is proposed here. By an electroplating-based surface machining process, the released nickel structure with the hinge mechanism can be fabricated. Lifting of the released micro structure to different tilted angles is accomplished by controlling the positions of a magnet beneath the device. An *in situ* electro-thermal actuator is used here to provide the pressing force in micro resistance welding for immobilizing the tilted structure. The proposed technique is shown to immobilize micro devices at controlled angles ranging from 14° to 90° with respect to the substrate. Design parameters such as the electro-thermal actuator and welding beam width are also investigated. It is found that there is a trade-off in beam width design between large contact pressure and low thermal deformation. Different dominated effects from resistivity enhancement and contact area enlargement during the welding process are also observed in the dynamic resistance curves. Finally, a lifted and immobilized electro-thermal bent-beam actuator is shown to displace upward about 27.7 μm with 0.56 W power input to demonstrate the capability of electrical transmission at welded joints by the proposed 3D micro assembly technique.

(Some figures in this article are in colour only in the electronic version)

1. Introduction

Three-dimensional (3D) micro assembly has been developed to provide more versatile micro structures for the performance enhancement of micro devices or systems, such as inductors [1], the hot-wire anemometer [2], flow sensors [3], the microcage [4] and the free-space micro-optical bench [5].

Lifting and immobilization of micro structure are two necessary functions usually involved in 3D micro assembly. Many approaches have been proposed for lifting micro structures, such as the pick-and-place technique [6, 7], electrostatic attraction [8, 9], residual stresses [10, 11], compliant mechanism [12], magnetic force [13, 14], and thermokinetic actuation [15], For immobilizing micro structures, these approaches usually included locking mechanisms [6–15].

Beside two-step approaches, some methods combined both lifting and immobilization in one step, including surface tension techniques [16–18], thermal shrinkage of polyimide [19], localized induction welding [20] and plastic deformation by the magnetic force [21]. For example, surface tension-based technology attains 3D micro assembly by heating materials to the liquid phase, then surface tension can act as a driving force to lift a released micro structure due to the minimization of the surface energy. Immobilization is then achieved after cooling. The assembled angle is designed by controlling the dimension of molten materials before the assembly process. For the plastic deformation approach, in order to implement plastic deformation, the angular displacement has to be large enough to exceed the elastic limit of the material. Assembly at a small tilted angle would not be easy, and the relaxation of the plastic deformation would also affect its angle. In general, these

[1] Author to whom any correspondence should be addressed.

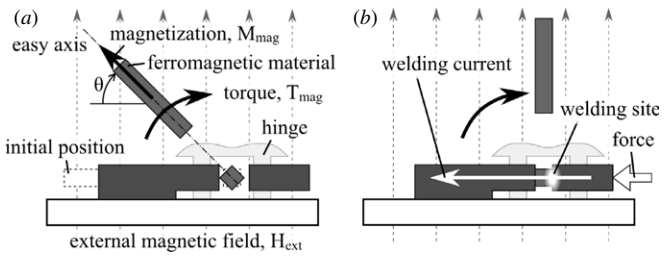

Figure 1. Illustration of the proposed 3D micro assembly concept. (*a*) Lifting of hinged Ni structure by the magnetic field. (*b*) Immobilization by micro resistance welding.

one-step approaches could only achieve limited angular range and tilted angle control. Using either two-step or one-step approaches in 3D micro assembly, electrical connection to the substrate is possible when the linking material is electrically conductive [1, 6, 7, 12, 17, 19, 20].

Welding is a common assembly process used in the macro scale by melting certain amount of materials between two workpieces. Among different welding technologies, resistance welding is a solder-free approach, needing no additional material between two workpieces. The principle of resistance welding is based on joule heating at the contact point due to its high contact resistance while pressing two workpieces together with current passing through. In our previous investigation [22], micro resistance welding for planar micro assembly using an *in situ* electro-thermal actuator was demonstrated, where the feasible operation conditions were also identified.

Here, by further incorporating a hinge mechanism and magnetic force, micro resistance welding with an *in situ* electro-thermal actuator for 3D micro assembly of the nickel micro device is proposed. The angular displacement can be actively adjusted by altering the position of the magnet beneath the device. Micro resistance welding with the assistance of electro-thermal actuators can fuse the welding region to immobilize the lifted micro structures. The welding characteristic and the angle tilting effect are investigated. Furthermore, an active micro device will be lifted, assembled and tested to demonstrate the electrical transmission capability in the proposed 3D micro assembly technique.

2. Operation principle

Figure 1 illustrates the proposed 3D micro assembly concept, where the hinged nickel micro structure is lifted by a magnetic force and fixed by micro resistance welding. Principles of magnetic actuation and resistance welding are introduced briefly in this session.

2.1. Magnetic lifting

The behavior of a ferromagnetic material in a magnetic field can be explained by the concept of magnetic anisotropy [23, 24]. With an external static magnetic field, $\vec{H}_{ext}$, applied perpendicularly to the substrate, as shown in figure 1(*a*), a piece of ferromagnetic material, such as a nickel film, can develop a magnetization, $\vec{M}_{mag}$, which interacts with $\vec{H}_{ext}$, to induce a torque $\vec{T}_{mag}$ acting on the nickel structure. A specific direction (easy axis) of magnetization in the material could be stronger than other directions. Because the low-stress electroplated nickel film is polycrystalline and the thickness of a thin film is much smaller than the other linear dimension, the magnetization will lie in the plane of the film. Therefore, the magnitude of the magnetic torque on a nickel film can be expressed as

$$|\vec{T}_{mag}| = |V(\vec{M}_{mag} \times \vec{H}_{ext})| = V \cdot M_{mag} \cdot H_{ext} \cdot \cos\theta \quad (1)$$

where V is the volume of the ferromagnetic material and θ is the angle between easy axis and the substrate, as shown in figure 1(*a*). The torque will become zero when the direction of easy axis aligns with the magnetic field direction, i.e. $\theta = 90^\circ$ in the case shown in figure 1(*a*). By changing the direction of the external magnetic field, it is possible to rotate the nickel film at different angles.

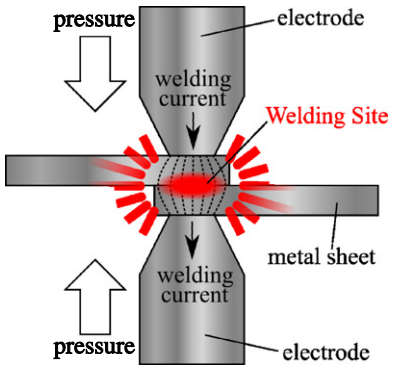

Figure 2. Illustration of the resistance welding.

2.2. Micro resistance welding

Resistance welding is used extensively in macro scale assembly, which consists of the material fusion at contact surfaces by the joule heating when the welding current runs through the workpieces. As illustrated in figure 2, providing a proper contact pressure by pressing two electrically conductive workpieces together leads to high contact resistance at the contact region because of the existence of asperities on the contact surface. When the welding current is running through contact points, temperature at the contact region is raised due to joule heating for a confined volume to the melting state. In general, a proper contact pressure is needed during the whole welding process. After switching off the welding current, the molten region gradually cools down until it has adequate mechanical strength.

The amount of generated heat can be expressed in terms of voltage, current and welding time as

$$Q = V_W \cdot I_W \cdot t = I_w^2 \cdot R \cdot t \quad (2)$$

where Q represents the heat generated, V_W the welding voltage, I_W the welding current, R the resistance at the interface or contact resistance and t the welding time.

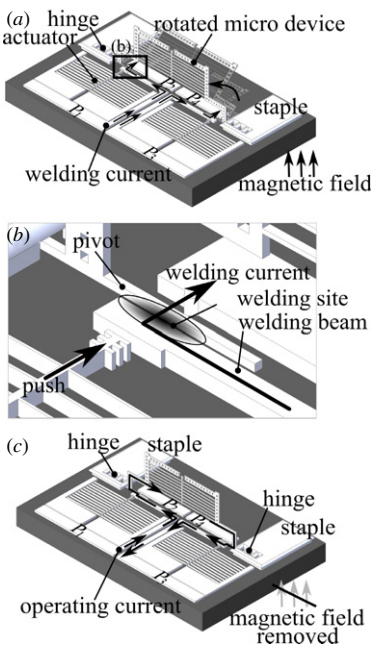

Figure 3. Illustrations of the structure design for the proposed 3D micro assembly. (*a*) Micro resistance welding with the electro-thermal actuator under magnetic lifting. (*b*) A close-up view of the welding site. (*c*) Applying the driving voltage to the assembled micro device from P_1 to P_3 through welded joints.

In our previous study [22], high contact pressure and welding energy were found to be critical to achieve a successful micro resistance welding. High contact pressure by the micro actuator leads to low initial contact resistance. For a given voltage, it will result in an increasing electrical current passing through the welding site, which produces more welding energy for a stronger welding joint.

3. Concept design

A sketch of the proposed configuration to accomplish 3D assembly is shown in figure 3(*a*). Components include staples, a hinged Ni micro structure to be lifted by the magnetic force and *in situ* electro-thermal actuator on the substrate for micro resistance welding.

The hinged micro structure could be an active device, such as a micro sensor or an actuator, rather than a simple flap. The *in situ* electro-thermal actuator to assist micro resistance welding here is composed of two arrays of parallel connected bent-beam actuators [25, 26], as shown in figure 3(*a*). In addition to these components, a welding beam is designed between the apex of the electro-thermal actuator and the pivot of the hinged micro device for the welding current to pass from pad P_1 to P_2 or P_3 to P_4 under contact pressure (figures 3(*a*) and (*b*)). It will fuse with the pivot beam together to form the welding joint and also prevent the apex of the actuator from being welded to the pivot. Welding beam could bear electrical current not only during welding process but also after the assembly when the lifted device needs to be applied operating voltage. Welding beam width is an important design parameter. A narrow welding beam has a low spring constant, which will need less force from actuator to push to contact with the pivot. However, a narrow welding beam also may induce large thermal stress during resistance welding.

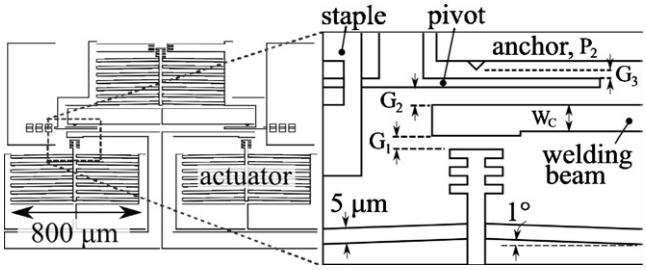

Figure 4. Illustration of geometric parameters around the welding site, including the gaps (G_1, G_2 and G_3) and the width (W_C) of the welding beam.

The procedure to accomplish the proposed 3D assembly can be described in following steps. An external magnetic field is first established by a permanent magnet, and then the hinged Ni micro device is magnetized and rotated away from the substrate to the desired position, depending on the direction of the external magnetic field passing through the hinged Ni device. Next, the electro-thermal actuator pushes the welding beam to have contact with the pivot beam of the lifted device. Under a proper contact pressure, the welding voltage is applied between P_1 and P_2, as well as P_3 and P_4, respectively. The welding current flows through the welding site (figure 3(*b*)) and generates heat for micro resistance welding. After a period of time, the welding voltage is turned off to cool down, and then the contact pressure is released to complete the 3D assembly. After assembly is complete, the metal welding joints would allow the electrical current passing through to operate the assembled micro device by applying the driving voltage between P_1 and P_3, as shown in figure 3(*c*).

4. Dimension design

In order to ensure enough contact pressure and displacement for micro resistance welding, the number and the dimension of bent beams in the parallel connected actuators have to be designed first.

In this study, the displacement requirement on actuators depends on the gaps (G_1, G_2 and G_3) around the welding region shown in figure 4. Considering our fabrication capability, the gaps G_1, G_2 and G_3 are determined to be 8 μm, 8 μm and 5 μm, respectively. The minimum required apex displacement of the actuator becomes the summation of these gaps, 21 μm. That means the apex of the actuator has to move forward at least 21 μm to push the suspended welding beam and the floating pivot beam to contact with the anchor P_2. Beside displacement requirement, the actuator also has to overcome the mechanical resistance, i.e. spring force from the suspended welding beam. Here, the thickness of the welding beam as well as bent-beam actuators is set to be 10 μm, and the effective suspended length of welding beams is 401 μm. Three different welding beam widths W_C, 4 μm, 11 μm and 30 μm, are designed, where the corresponding spring constants of welding beams are 0.5, 10.6 and 216 N m^{-1}.

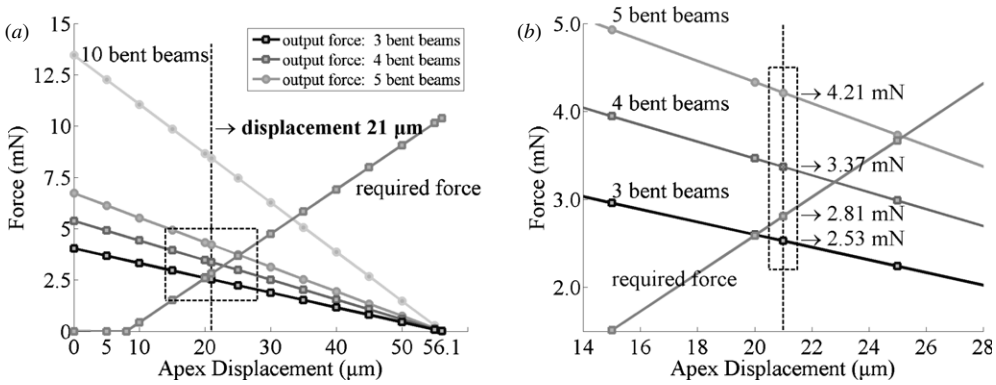

Figure 5. (*a*) Output forces at different displacements of the apex with different numbers of bent beams, as well as the required force at two operation stages. (*b*) The enlargement of the region around the 21 μm apex displacement.

Table 1. Material properties of nickel adopted in finite element analysis.

Modulus of elasticity (GPa)	207
Density (kg m^{-3})	8880
Coefficient of thermal expansion (10^{-6} K^{-1})	12.7
Poisson ratio	0.31
Thermal conductivity (W m^{-1} K^{-1})	90.5
Specific heat (J kg^{-1} K^{-1})	443
Resistivity (10^{-8} Ωm)	13.5

The actuator performance can be altered by changing the geometry of the bent beam [22, 25, 26]. The stroke can be increased by designing a longer beam, and the output force is proportional to the number of bent beams in the parallel connected actuator.

The stroke of actuator can be divided into two stages. When the apex displacement of the actuator travels from 0 μm to 8 μm, it moves without mechanical resistance. When it proceeds from 8 μm to 21 μm, the actuator has to overcome the mechanical resistance from the stiffness of the welding beam. In fact, an even larger force is preferred to provide higher contact pressure for better micro resistance welding [22].

A finite element model on the bent-beam actuator is built here to simulate the output displacements and the output forces with different numbers of bent beams in the parallel connected actuator. The material properties of nickel adopted in the finite element analysis is listed in table 1 [27]. Some dimensions (thickness of the bent beam 10 μm, beam width 5 μm, total bent-beam length 800 μm and bent angle 1°) are adopted from our previous study [22]. In simulations, the highest temperature is limited to 400 °C to prevent degeneration of nickel. The performance of the bent-beam actuator resulting from finite element analysis is given in figure 5 where the required force is calculated with the largest spring constant, 216 N m^{-1}. The output force decreases with the increasing output displacement and increases with the increasing number of bent beams in the parallel connected actuators, as shown in figure 5. The minimum required force is 2.81 mN at a displacement of 21 μm for a spring constant of 216 N m^{-1}. Figure 5(*b*) indicates that at least four bent beams are needed to meet the minimum force requirement. For further ensuring sufficient force for high contact pressure, design with 20 bent beams is used here in the parallel connected bent-beam actuator.

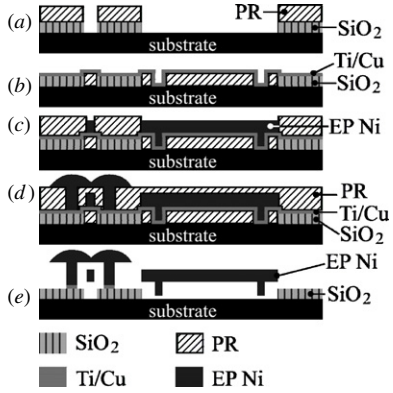

Figure 6. Fabrication process of the devices.

5. Fabrication

The micro structures described above are fabricated by the metal-based surface micro machining technique with two electroplating steps for the 10 μm thick nickel micro structure and the mushroom-like staple. The fabrication process is illustrated in figure 6. In the beginning, oxide thin film is grown and patterned using the first mask by HF wet etching (figure 6(*a*)). Next, FH 6400 photoresist (PR) is coated and patterned to act as the sacrificial layer, and then a Ti/Cu thin film of 120/20 nm is deposited as the adhesion and seed layer, as shown in figure 6(*b*). Another 15 μm thick AZ 10XT photoresist is coated and patterned to serve as the electroplating mold. A 10 μm thick nickel is then electroplated (EP) to form the metal structure (figure 6(*c*)). After removing the electroplating mold, another AZ 10XT photoresist is coated and patterned, and the second electroplating process is employed to fabricate the staples (figure 6(*d*)). The AZ 10XT photoresist is adopted here to be the spacer and sacrificial layer. At the second electroplating step, the extended electroplating time makes the nickel overflow the mold to form a mushroom-like shape. In this way, the hinge can be fabricated in one step. Finally, after removing the photoresist and the adhesion/seed layer by wet etching (figure 6(*e*)), the structure is dipped in

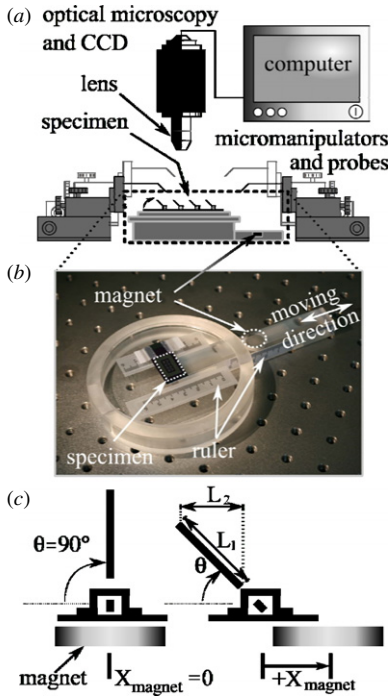

Figure 7. (*a*) Illustration of the experimental setup. (*b*) PMMA holder with a movable magnet beneath the specimen. (*c*) Different tilted angle by changing the lateral position of the magnet.

isopropyl alcohol (IPA) and heated on a 65 °C hot plate to release.

6. Testing

The experimental setup for the proposed 3D micro assembly includes a probe station with a computer and a custom-made specimen holder made of polymethyl methacrylate (PMMA), as shown in figure 7(*a*). Devices with three different widths on welding beam, W_C (4 μm, 11 μm and 30 μm), are tested. During the welding process, the values of the welding current and welding voltage can be retrieved from a computer-controlled power supply.

The fabricated micro structure (specimen) is first put on the top of the holder where a movable circular magnet of 15 mm in diameter with a magnetic field of 250 kA m^{-1} measured by a gaussmeter (model 5100, Sypris Test & Measurement Inc.) is placed about 5 mm beneath the specimen, as shown in figure 7(*b*). By changing the lateral position of the magnet along the rail underneath the specimen, the direction of the magnetic field passing through the specimen can be altered, which would rotate the released nickel structure at different angles, as illustrated in figure 7(*c*). When the magnet is kept right beneath the device, i.e. $X_{\text{magnet}} = 0$, it will keep the device at the up-right position, i.e. 90°. For different magnet positions, the device can rotate between 0° and 180°. When the device is kept at the specified angle by the magnet field, the micro resistance welding is then processed. It follows three steps in resistance welding: press, weld and release. The electro-thermal actuator with about 1.2 W input power (at 1.6 V) will push the suspended welding beam and the pivot to contact with the anchor P_2. Under the contact pressure, the dc welding voltage gradually increases to 1.5 V and the welding current passes through the welding site from the anchor P_1 via the welding beam and pivot beam to P_2, as illustrated in figure 3(*a*). After 150 s, the welding voltage is gradually turned off to cool down the welding site. Then, the contact pressure is released by turning off the electro-thermal actuator. After completing the micro resistance welding, the magnet can be removed. Additionally, by applying the voltage between anchors P_1 and P_3, the resistance of the welded joints after assembly can be examined. Tilted angle measurement before welding is based on images taken by the CCD camera. By measuring length L_1, and projected length, L_2, of the lifted device (figure 7(*c*)) from the captured image, tilted angle, θ, can be calculated. The resolution of images captured by CCD camera is 3 μm per pixel. For a 400 μm-long (L_1) device, the corresponding angular resolution is about 0.5°. For determining tilted angles after welding, similar calibrations are performed, except the images come from SEM pictures.

7. Results and discussions

By moving the magnet under the holder closer or away from the specimen, the hinged Ni micro device can be lifted to different positions. The relation between the magnet position and the tilted angle before micro resistance welding is shown in figure 8, where $X_{\text{magnet}} = 0$ is defined at the position right beneath the specimen with a tilted angle about 90°. All data are measured with the same device to rotate multiple times at different magnet positions. For each magnet position, the tilted angle is measured three times. By assuming that the tilted angle represents the resultant magnetic field direction, figure 8 could also be considered as experimental results describing the resultant magnetic field directions on the hinged Ni structure at different magnet positions. It is shown that the lifted angle can be changed from 10.5° to 175° when X_{magnet} is from +12 mm to −12 mm, respectively. Once the magnet is placed further than 12 mm in a positive or negative direction, tilted angles up to 0° or 180°, respectively, can also be achieved. However, when the device is rotated near 180°, the device will touch another structure anchored on the substrate. The floating pivot beam will then be lifted upward due to the thickness of the touched structure, so the pivot beam and welding beam may not be on the same plane completely. Furthermore, during resistance welding, the lateral force from the actuator will push the tilted pivot beam to rotate, and this also makes precise immobilization close to 0° and 180° more difficult.

Figure 9 shows the photographs around the welding site at three operating states during the proposed 3D micro assembly. After placing the specimen on the holder (figure 9(*a*)), the micro device is lifted first, then the electro-thermal bent-beam actuator pushes the welding beam to contact with the floating pivot beam (figure 9(*b*)). The actuator is released from the welding beam once the micro resistance welding is done (figure 9(*c*)). Typical assembled results are shown in figure 10, where three micro devices on the same wafer are assembled at three different tilted angles, 14°, 35° and 90°. The deviation on tilted angles before and after micro resistance is found to be around 2.5°–4°

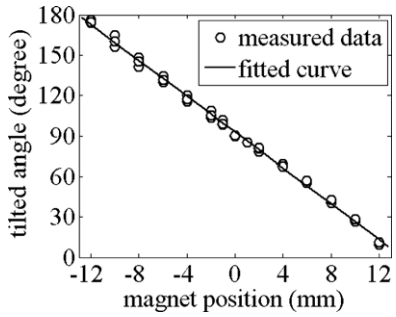

Figure 8. Relation between magnet positions and tilted angles before micro resistance welding.

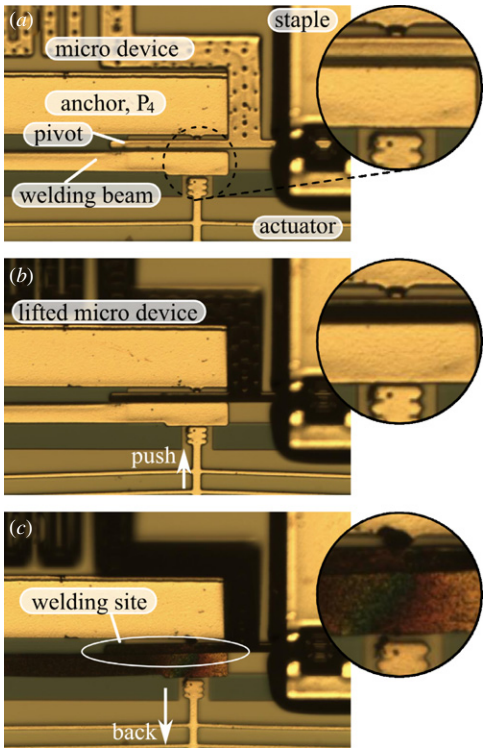

Figure 9. Photographs around the welding site during the proposed 3D micro assembly. (*a*) Initial configuration; (*b*) actuator pushes the welding beam to contact with the pivot to generate contact pressure; (*c*) actuator is released after a successful micro resistance welding.

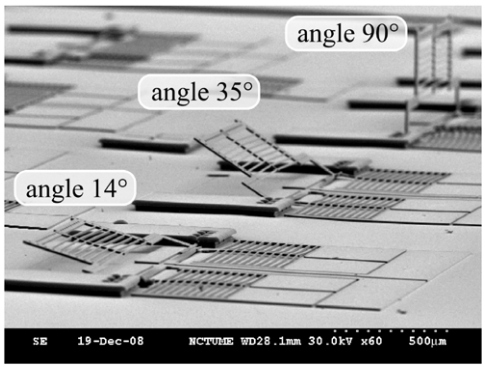

Figure 10. SEM picture on assembled micro devices at different tilted angles (14°, 35° and 90°).

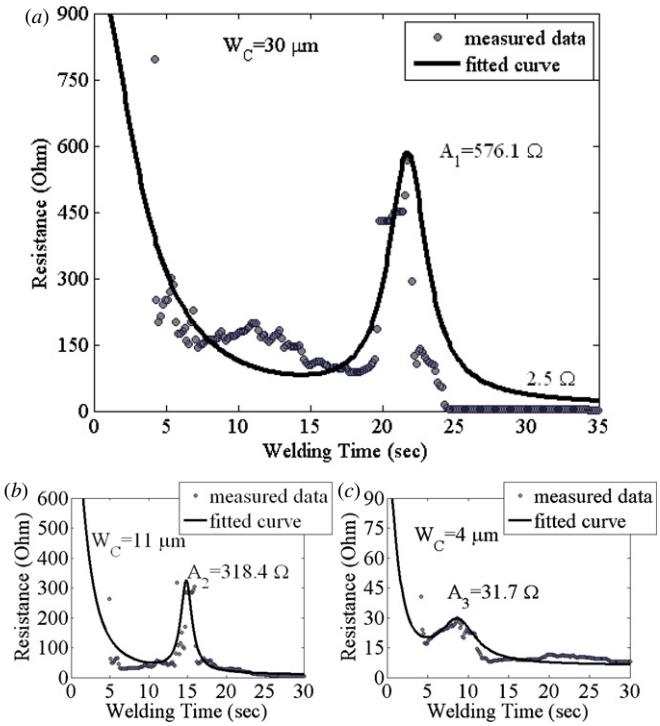

Figure 11. Dynamic resistance curves from different welding beam widths: (*a*) $W_C = 30\ \mu$m, (*b*) $W_C = 11\ \mu$m and (*c*) $W_C = 4\ \mu$m.

The instantaneous resistance, or dynamic resistance, during the welding process is recorded. Dynamic resistance is defined as the instantaneous voltage divided by instantaneous current. Typical dynamic resistance curves measured in this study are shown in figure 11 while assembling the lifted devices at 90° positions. The pattern of these curves can be explained as follows [28, 29].

In the beginning, asperities exist on the contact surface because of surface roughness. When workpieces are brought in contact with each other, electrical paths through some micro contact points are created. However, the oxide layer or contaminants would be also presented on the contact surface under normal circumstances. Those insulators could cause very high initial resistance at the early stage. When the welding voltage is gradually increased, the breakdown of the surface allows more current passing through the micro contact points. Temperature around these micro contact points is then raised to soften the asperities and increase the contact area, which results in dynamic resistance decreasing. However, the resistivity will also increase with the increasing temperature. The dynamic resistance will reach a local minimum value and then start increasing to a maximum value when the resistivity enhancement effect is stronger than the contact area enlargement effect. As the heating progresses, more volume of the metal around the contact region will be melted, the so-called mechanical collapse and nugget growing. When the temperature is stabilized, the dynamic resistance will fall from the peak value A_1 to a stable value due to the domination of the mechanical collapse and nugget growing effect, as shown in figure 11(*a*), for example, at welding time around 22 s.

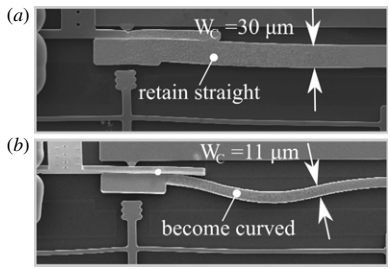

Figure 12. Pictures of the welding beams after welding with different widths: (*a*) $W_C = 30$ μm and (*b*) $W_C = 11$ μm.

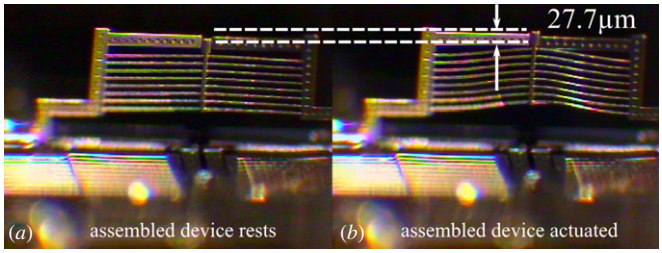

Figure 13. Testing on an assembled micro actuator. (*a*) Initial state. (*b*) The apex travels 27.7 μm upward subjecting to the electrical power 0.56 W.

Dynamic resistance curves from different welding beam widths are also shown in figure 11. It is found that the local maximum value (A_1, A_2 and A_3) in dynamic resistance curves decreases with the beam width, W_C, under the same welding voltage 1.5 V. A wider welding beam means more mechanical resistance to the actuator. The output force of the actuator needs to overcome this mechanical resistance first; then the remaining force provides the contact pressure to the welding site. Under the same actuator output force and displacement, a narrower welding beam leads to a higher contact pressure, which produces a more intimate contact. Consequently, the local maximum value of the dynamic resistance curve is smaller. However, a narrow welding beam would suffer large thermal stress during welding. As shown in figure 12(*b*), evident thermal deformation is observed in the cases with an 11 μm beam width. Comparatively, the 30 μm beam still retains its straight shape. There is a trade-off in welding beam width. A narrow beam is good for actuator to provide high contact pressure; however, it may cause unexpected deformation due to the thermal stress.

For assembling hinged devices at different angles with the same welding beam width, no significant difference is found in the dynamic resistance curves. Since the side wall is not perfectly vertical after fabrication, the cross section of the electroplated beam becomes an upside-down trapezoid. Therefore, the contact between the pivot beam and welding beam is more like a line contact rather than a surface-to-surface contact while pressing together by the actuator. In other words, even at different tilted angles, the contact area won't change significantly due to the line-contact condition. Therefore, it may have similar dynamic curves at different tilted angles.

In this work, the space in hinge structure is designed to be large enough to prevent the micro structure from getting jammed [9]. In our experiments, structures getting jammed or stuck during lifting was not found. However, stiction did happen in fabrication due to the wet releasing process. In our fabrication capability, at least 6 out of 8 test samples can be released successfully on a single die. Once the device is released successfully, all devices can be reliably rotated to the desired angle with the corresponding magnet position.

An active micro device, the electro thermal bent-beam actuator, is lifted, assembled and tested here. By applying electrical power 0.56 W, the assembled actuator displaces 27.7 μm in the out-of-plane direction, as shown in figure 13, which further verifies the electrical transmission capability at welded joints by the proposed 3D micro assembly technique.

8. Conclusions

A 3D micro assembly technique has been proposed and implemented here. With magnetic lifting and micro resistance welding, the hinged Ni devices are shown to be lifted and immobilized in a wide-range tilted angle successfully. Design issues such as the micro actuator configuration and welding beam width are investigated. It is found that there is a trade-off in beam width design between high contact pressure and low thermal deformation. Different dominated effects between resistivity enhancement and contact area enlargement during the welding process are also observed in the dynamic resistance curves. The proposed assembly technique not only can provide electrical connecting capability at welded joints, but also may be helpful in the automation of 3D micro assembly.

Acknowledgments

This work was supported by the National Science Council (Taiwan) under grant NSC 95-2221-E009-012-MY2. The authors also would like to express their appreciation to the Nano Facility Center of National Chiao Tung University for providing facilities and technical support.

References

[1] Zou J, Liu C, Trainor D R, Chen J, Schutt-Ainé J E and Chapman P L 2003 Development of three-dimensional inductors using plastic deformation magnetic assembly (PDMA) *IEEE Trans. Microw. Theory Tech.* **51** 1067–75

[2] Chen J and Liu C 2003 Development and characterization of surface micromachined, out-of-plane hot-wire anemometer *J. Microelectromech. Syst.* **12** 979–88

[3] Fan Z, Chen J, Zou J, Bullen D, Liu C and Delcomyn F 2002 Design and fabrication of artificial lateral line flow sensors *J. Micromech. Microeng.* **12** 655–61

[4] Ok J, Lu Y-W and Kim C-J 2006 Pneumatically driven microcage for microbe manipulation in a biological liquid environment *J. Microelectromech. Syst.* **15** 1499–504

[5] Wu M C, Lin L-Y, Lee S-S and Pister K S J 1995 Micromachined free-space integrated micro-optics *Sensors Actuators* A **50** 127–34

[6] Tsui K, Geisberger A A, Ellis M and Skidmore G D 2004 Micromachined end-effector and techniques for directed MEMS assembly *J. Micromech. Microeng.* **14** 542–49
[7] Mayyas M, Zhang P, Lee W H, Popa D and Chiao J C 2009 An active micro joining mechanism for 3D assembly *J. Micromech. Microeng.* **19** 035012
[8] Johnstone R W and Parameswaran M 2001 Self-assembly of surface-micromachined structures using electrostatic attraction *Proc. SPIE* **4561** 66
[9] Ardanuc S, Lal A and Reyes D 2007 Process-independent, ultrasound-enhanced, electrostatic batch assembly *14th Int. Conf. on Solid State Sensors and Actuators (TRANSDUCERS '07)* (Lyon, France: IEEE) pp 407–10
[10] Li L, Zawadzka J and Uttamchandani D 2004 Integrated self-assembling and holding technique applied to a 3-D MEMS variable optical attenuator *J. Microelectromech. Syst.* **13** 83–90
[11] Johnstone R W, Sameoto D and Parameswaran M 2006 Non-uniform residual stresses for parallel assembly of out-of-plane surface-micromachined structures *J. Micromech. Microeng.* **16** N17–N22
[12] Tsang S-H, Sameoto D, Foulds I G, Johnstone R W and Parameswaran M 2007 Automated assembly of hingeless 90° out-of-plane microstructures *J. Micromech. Microeng.* **17** 1314–25
[13] Yi Y W and Liu C 1999 Magnetic actuation of hinged microstructures *J. Microelectromech. Syst.* **8** 10–7
[14] Iwase E and Shimoyama I 2005 Multistep sequential batch assembly of three-dimensional ferromagnetic microstructures with elastic hinges *J. Microelectromech. Syst.* **14** 1265–271
[15] Kaajakari V and Lal A 2003 Thermokinetic actuation for batch assembly of microscale hinged structures *J. Micromech. Microeng.* **12** 425–32
[16] Harsh K F, Bright V M and Lee Y C 1999 Solder self-assembly for three-dimensional microelectromechanical Systems *Sensors Actuators* A **77** 237–44
[17] Syms R R A 1998 Rotational self-assembly of complex microstructures by the surface tension of glass *Sensors Actuators* A **65** 238–43
[18] Syms R R A 1999 Surface tension powered self-assembly of 3-D micro-optomechanical structures *J. Microelectromech. Syst.* **8** 448–55
[19] Ebefors T, Kalvesten E and Stemme G 1998 New small radius joints based on thermal shrinkage of polyimide in V-grooves for robust self-assembly 3D microstructures *J. Micromech. Microeng.* **8** 188–94
[20] Yang H-A, Lin C-W and Fang W 2006 Wafer level self-assembly of microstructures using global magnetic lifting and localized induction welding *J. Micromech. Microeng.* **16** 27–32
[21] Zou J, Chen J, Liu C and Schutt-Ainé J E 2001 Plastic deformation magnetic assembly (PDMA) of out-of-plane microstructures: technology and application *J. Microelectromech. Syst.* **10** 302–09
[22] Chang C-W, Yeh C-C and Hsu W 2009 Experimental investigation and characterization of micro resistance welding with an electro-thermal actuator *J. Micromech. Microeng.* **19** 025001
[23] Soohoo R F 1965 *Magnetic Thin Films* ed F Seitz (New York: Harper & Row) pp 27–36
[24] Judy J W and Muller R S 1997 Magnetically actuated, addressable microstructures *J. Microelectromech. Syst.* **6** 249–56
[25] Que L, Park J-S and Gianchandani Y B 2001 Bent-beam electrothermal actuators: Part I. Single beam and cascaded devices *J. Microelectromech. Syst.* **10** 247–54
[26] Sinclair M J 2000 A high force low area MEMS thermal actuator *Proc. 7th Intersociety Conf. on Thermal Phenomena (Las Vegas, NV)* vol 1 pp 127–32
[27] Hsu C-P, Liao T and Hsu W 2003 Electrothermally-driven long stretch micro drive with monolithic cascaded actuation units in compact arrangement *12th Int. Conf. on Solid-State Sensors, Actuators and Microsystems (TRANSDUCERS'03) (Boston, MA)* vol 1 pp 8–12
[28] Savage W F, Nippes E F and Wassell F A 1978 Dynamic contact resistance of series spot welds *Weld. J.* **57** 43s–50s
[29] Bickinson D W, Franklin J E and Stanya A 1980 Characterization of spot welding behavior by dynamic electrical parameter monitoring *Weld. J.* **59** 170s–6s